Converse magnetoelectric experiments on a room-temperature spirally ordered hexaferrite

Khabat Ebnabbasi* and Carmine Vittoria
Department of Electrical and Computer Engineering, Northeastern University, Boston, Massachusetts 02115, USA

Allan Widom
Physics Department, Northeastern University, Boston, Massachusetts 02115, USA

(Received 28 November 2011; revised manuscript received 21 June 2012; published 25 July 2012)

Magnetoelectric properties of room-temperature spirally ordered $Sr_3Co_2Fe_{24}O_{41}$ hexaferrite slabs have been measured. A physical model in this paper referred to as the "slinky helix" model is presented to explain the experimental data. The measured properties include the magnetic permeability and the strain, all as a function of the electric field **E**. Upon application of an electric field to slabs of Sr Z-type hexaferrite, it exhibits broken symmetries for time reversal and parity. This is the central feature of these magnetoelectric materials.

DOI: 10.1103/PhysRevB.86.024430 PACS number(s): 75.85.+t, 75.30.−m, 84.40.−x, 85.75.−d

I. INTRODUCTION

There has been considerable recent interest in the nature of magnetoelectric (ME) materials.[1] Of interest in this work is spirally ordered hexaferrites,[2–5] which have strong ME effects at room temperature. Neutron scattering experiments[5,6] revealed a spiral spin configuration responsible for the ME effect at room temperature in $Sr_3Co_2Fe_{24}O_{41}$ hexaferrite. $Sr_3Co_2Fe_{24}O_{41}$ is identified as a Z-type hexaferrite consisting of S, R, and T "spinel" blocks.[4,5] It was further revealed that in the T block the Fe-O-Fe bond angles were slightly deformed to affect the superexchange interaction between the Fe ions and induce the spiral spin configuration[7] in $Sr_3Co_2Fe_{24}O_{41}$ as shown in Fig. 1. Changes in the spin spiral configuration in the presence of an electric field **E** induce changes in the magnetization **M**. In a polycrystalline sample such as ours it induces changes in the remanent magnetization. This physical mechanism for the ME effect is very different from the mechanisms applicable to multiferroic materials in the past. This new mechanism opens up new properties or opportunities in the physics and applications of ME materials.

The previously most used technique to explore ME effects was ferromagnetic resonance (FMR). In the past FMR frequency shifts were measured with an applied **E**. There has never been a report on permeability measurement in ME material with application of an electric field, although there are many reports on FMR shifts. The measurement of FMR frequency shifts is ineffectual in our case, because (a) the shifts are extremely small and (b) they are strongly damped in the new mechanism. Hence, we have devised a new measurement method whereby the permeability of our material is measured directly via a modified coaxial line technique. We refer to these measurements as "converse" ME measurements.

Although previous authors[1–5] have established a strong correlation between the spiral configuration and the ME effect, we provide a physical picture, i.e., model for the effect. Our measurements reveal that $Sr_3Co_2Fe_{24}O_{41}$ is electrostrictive. As such, the application of **E** strains the material, thereby changing the physical structure of the spiral spin configuration. It is this physical motion of the spiral response to **E** that induces a change in magnetization **M**. We refer to this model as the "slinky helix" model. Our model should be contrasted with the model for the ME effect in multiferroics as well as ferromagnetic metal films wherein the band energies of the up and down spin are modified by the electric fields at the interface between phase separated ferromagnetic and ferroelectric films. The change in band splitting leads to a change in surface magnetization.[8]

The thermodynamic enthalpy per unit volume $w(s,\mathbf{E},\mathbf{H},\boldsymbol{\sigma})$ determines all of the spirally ordered hexaferrite thermodynamic equations of state[9] via the thermodynamic minimum principle:

$$w(s,\mathbf{E},\mathbf{H},\boldsymbol{\sigma}) = \min_{\mathbf{P},\mathbf{M}}[\tilde{w}(s,\mathbf{P},\mathbf{M},\boldsymbol{\sigma}) - \mathbf{E}\cdot\mathbf{P} - \mathbf{H}\cdot\mathbf{M}]$$
$$dw = T\,ds - \mathbf{P}\cdot d\mathbf{E} - \mathbf{M}\cdot d\mathbf{H} - \mathsf{e} : d\boldsymbol{\sigma}. \tag{1}$$

Here, T, **P**, **M**, and e represent, respectively, the temperature, polarization, magnetization, and strain, while s, **E**, **H**, and $\boldsymbol{\sigma}$ represent, respectively, the entropy per unit volume, electric field, magnetic intensity, and stress. Other thermodynamic quantities of interest include the adiabatic dielectric constant tensor

$$\boldsymbol{\epsilon} = \mathbf{1} + 4\pi\left(\frac{\partial\mathbf{P}}{\partial\mathbf{E}}\right)_{s,\mathbf{H},\boldsymbol{\sigma}} = \mathbf{1} + 4\pi\,\boldsymbol{\chi}_{\mathbf{P}}, \tag{2}$$

the adiabatic permeability tensor

$$\boldsymbol{\mu} = \mathbf{1} + 4\pi\left(\frac{\partial\mathbf{M}}{\partial\mathbf{H}}\right)_{s,\mathbf{E},\boldsymbol{\sigma}} = \mathbf{1} + 4\pi\,\boldsymbol{\chi}_{\mathbf{M}}, \tag{3}$$

and the adiabatic ME tensor

$$\boldsymbol{\alpha} = \left(\frac{\partial\mathbf{M}}{\partial\mathbf{E}}\right)_{s,\mathbf{H},\boldsymbol{\sigma}} = \left(\frac{\partial\mathbf{P}}{\partial\mathbf{H}}\right)_{s,\mathbf{E},\boldsymbol{\sigma}}. \tag{4}$$

Conventional experiments probing ME effects measure elements of the ME tensor $\alpha_{ij} = (\partial M_i/\partial E_j)_{s,\mathbf{H},\boldsymbol{\sigma}}$. In the converse experiments reported in this work, the ME effect is probed by measuring elements of the magnetic permeability tensor $\boldsymbol{\mu}$ and the strain tensor e, while noting the manner in which these tensors depend on **E** and **H**. Direct measurements of the magnetization **M** were also employed.

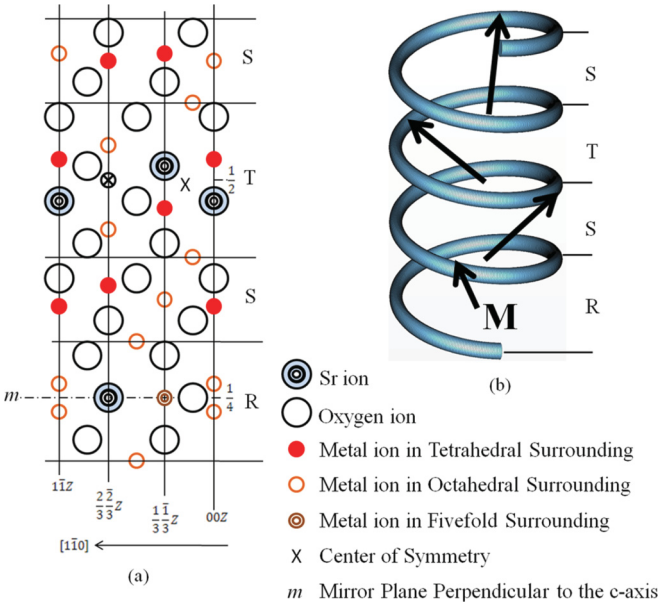

FIG. 1. (Color online) (a) Crystal structure of a part of the hexagonal unit cell. (b) Spiral spin order.

II. EXPERIMENTAL RESULTS

A. Experimental material growth and magnetoelectric measurement technique

We have adopted a procedure similar to that in Ref. 5 to prepare a single phase of $Sr_3Co_2Fe_{24}O_{41}$ except for the following preparation steps. In order to prevent the formation of other impurity phases, including W-, M- and/or Y-type phases, it was found most favorable to quench the sample immediately to room temperature after annealing. Our x-ray data are consistent with a Z-type hexaferrite structure.[11] Also, for the ME measurements it is important to minimize conductance current flow or heating effects through the sample in the presence of high electric fields. As such, the resistivity was increased by annealing the samples at 600 °C in an oxygen atmosphere for 6 h. The resistivity estimated from the experimental linear *I-V* characteristic was $\rho = 1.43 \times 10^9$ Ω-cm for samples of 1-mm thickness. The preparation in oxygen leads to an Fe^{2+} concentration reduction, which then lowers the hopping of electrons between Fe^{2+} and Fe^{3+} ions.[5,10] Typically, coaxial lines are used to measure permeability and dielectric constants as a function of frequency, but never in the presence of an electric field or a dc voltage as high as 2000 V. In order to minimize the risks to the instrumentation, the termination of the coaxial line was electrically separated from the rest of the coaxial line by ∼10 mil. Software was developed in order to calculate the effects of the separation on the measurement of μ. The technique was calibrated or standardized against well-known coaxial line results where the line was not split.

We inserted a toroidal-shaped sample in a coaxial line. One side of the toroid was shorted to the coaxial line termination as well as to the dc ground voltage. The other side of the toroid was coated with a thin film of silver paint and then connected to a high dc voltage power supply. Three precautions need to be exercised, as follows. (i) The high dc voltage must be isolated from the microwave voltage of network analyzer instrumentation. (ii) Antenna effects from dangling wires connected to the toroidal sample must be reduced. The vector network analyzer was used to measure the electrical scattering *S*-parameter. Antenna effects were reduced by connecting high-frequency capacitors to electrically short out any microwave signals in the dangling wires. (iii) Finally, the thickness of the silver paint film must be sufficiently small compared to the skin depth (10 μm < 200 μm) so that the reflected signal from the toroid is not dominated by pure metallic reflection from the silver paint. For example, initially we inserted the toroidal sample without any wire attachments, silver paint, or capacitors attached to any wire. In short, a conventional coaxial line measurement was performed to measure μ as a function of frequency (see Fig. 2). We then loaded the toroidal sample with all the attachments (wires, paint, capacitors, etc.) but no dc voltage applied and measured μ again. We were again able to obtain the same μ curve as in Fig. 2. At this point we applied the dc voltage to the toroidal sample so we measured changes in μ due to the dc voltage.

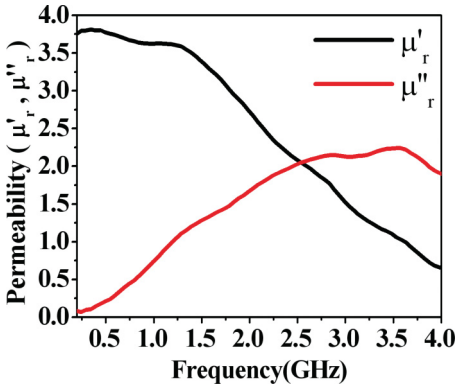

FIG. 2. (Color online) Real and imaginary parts of the polycrystalline Sr Z-type permeability versus frequency.

Using conventional scattering *S*-parameter analysis, μ may be calculated from the reflection coefficient, S_{11} (see Fig. 3). The analysis is simplified considerably if the thickness of the toroidal sample is less than the wavelength in the sample (1 mm ≪ 6 cm). The calculated S_{11} scattering coefficient was calculated as follows:[14]

$$S^s_{11} = \left(\frac{-Z_0\cos(kt) - iZ\sin(kt)}{Z_0\cos(kt) - iZ\sin(kt)}\right) - iZ\tan(kt)$$
$$= Z_0\left(\frac{1+S^s_{11}}{1-S^s_{11}}\right), \quad (5)$$

where $Z = \sqrt{\mu/\epsilon}$ and $k = \omega\sqrt{\mu\epsilon}$.

Here S^s_{11} is the reflection coefficient for the shorted port of the coaxial transmission line; Z is the coaxial line characteristic impedance of the sample; k is the propagation constant, which is equal to $2\pi/\lambda$; t is the sample thickness; and Z_0 is the characteristic impedance of the coaxial line, which is 50 Ω. The permeability may then be determined from

$$\mu \simeq Z_0\left(\frac{1}{-i\omega t}\right)\left(\frac{1+S^s_{11}}{1-S^s_{11}}\right), \quad (6)$$

where ω is $2\pi f$ and f is the frequency. Note that this formula is an approximate formula and it is valid as long as $kt \ll 1$. The

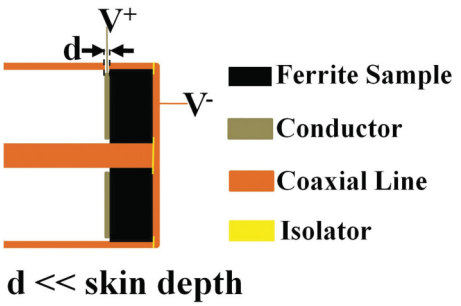

FIG. 3. (Color online) Coaxial line schematic.

sample thickness was 1 mm and the approximation is valid up to 3 GHz. The advantage of our approach or calculation technique is that the dielectric constant, ϵ, does not enter into the analysis in this limit of approximation. This is an extremely important point in that dielectric changes cannot influence the changes in μ as measured by this technique, as there is no dependence on ϵ in Eq. (6).

Microwave experiments were performed under the following conditions: For a given direction of the remanent magnetization, $\mathbf{M}_r$, the electric field was applied parallel, antiparallel, and perpendicular to $\mathbf{M}_r$. Prior to the experiments the remanence direction was poled with a permanent magnet. In Fig. 2, we illustrate the complex relative magnetic permeability $\mu(\omega + i0^+)$ for low microwave frequencies, on the scale of the ferromagnetic resonant frequency. In the limit $\omega \to 0$, we expect the permeability, $\mu(0)$, to be of the order of[14]

$$\mu(0) = 1 + \left(\frac{4\pi M_r}{H_\phi}\right), \tag{7}$$

where M_r is the remanence magnetization and H_ϕ is the six-fold magnetic anisotropy field. We measured $4\pi M_r = 105$ G and thereby $H_\phi \simeq 40$ Oe, as in Fig. 2. This result is typical of Z-type hexaferrite.[7] The permeability $\mu(\omega)$ as a function of the frequency is given as[14]

$$\mu(\omega) = 1 + \left(\frac{4\pi M_r H_1}{H_1 H_2 - \omega^2/\gamma^2}\right), \tag{8}$$

where $4\pi M_r$ is the remanence magnetization, $H_1 = H + H_\phi + 4\pi M_r + H_\theta$, H is the external magnetic field, H_ϕ is the six-fold magnetic anisotropy field, H_θ is the polar angle uniaxial magnetic anistropy field, $H_2 = H + H_\phi$, $\gamma = g(\frac{e}{2mc}) \simeq 1.4g \times 10^6$, and $g \simeq 2$.

Magnetic damping may be included by making ω complex. For example, $(\frac{\Delta\omega}{\gamma}) \simeq 100$ Oe at X-band frequencies for Z-type hexaferrites, where $\omega \to \omega + i\Delta\omega$ (magnetic damping). For $H > 0$ such that magnetization saturation occurs, $4\pi M_r$ is replaced by $4\pi M_s$, M_s saturation magnetization. In our experiments $H = 0$ and thus there is no magnetic saturation. All of the magnetic parameters in Eq. (8) were measured by us in Ref. 11. This means that for a given value of $4\pi M_r$, μ may be plotted as a function of frequency. The plot in Fig. 2 applies for $H = 0$ and $E = 0$. However, as E was varied in our experiment, $4\pi M_r$ also varied. This implies that from the knowledge of $4\pi M_r$ alone as determined at zero frequency, one may indeed infer μ as a function of frequency. Hence, a family of curves of μ versus frequency may be plotted where $4\pi M_r$ or E is the third variable parameter, since $4\pi M_r$ is related to E via

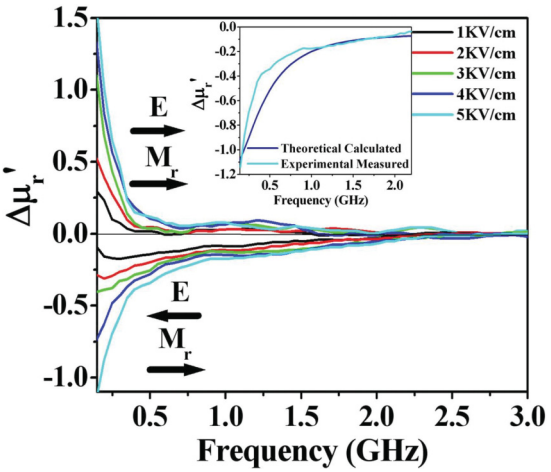

FIG. 4. (Color online) Magnetic permeability change versus electric field over a microwave frequency range when $\mathbf{M}$ is parallel and antiparallel to $\mathbf{E}$. Inset: Theoretical calculation and experimental measurement for $E = 5$ KV/cm.

the ME effect of these materials. This was an important clue in the performance of our experiment at microwave frequencies. We chose to measure the change in μ, $\Delta\mu$, relative to the value of μ at $E = 0$ and $H = 0$, as a function of frequency. We do not report the imaginary component of $\Delta\mu$, since there is no FMR line width measurement on these materials.

B. Experimental magnetoelectric measurements

Figures 4 and 5 show the change in permeability when an electric field is applied parallel or antiparallel and perpendicular to the magnetization, respectively. Under a change in parity, $\mathbf{E} \to -\mathbf{E}$ and $\mathbf{M}_r \to \mathbf{M}_r$. Under time reversal, $\mathbf{E} \to \mathbf{E}$ and $\mathbf{M_r} \to -\mathbf{M}_r$. The data indicate both a broken parity and a broken time reversal symmetry. This represents the fundamental broken symmetry expected of ME effects.

The measurements in Fig. 4 correlate very well with the vibrating sample measurements whereby $\mathbf{M_r}$ scales as $\mathbf{E}$, changing polarity with the direction of $\mathbf{E}$.[11] The quadratic ME interaction in the conjugate enthalpy of Eq. (1) is given by

$$\Delta\tilde{w} = \beta(\mathbf{n}\cdot\mathbf{M})(\mathbf{n}\cdot\mathbf{P}), \tag{9}$$

where $\mathbf{n}$ is a unit vector in along the spiral axis.

The total driving fields $\mathbf{E}_d$ and $\mathbf{H}_d$ have a reversible and an irreversible thermodynamic part.[12,13] There are two ways to calculate the change in μ with frequency and E. One way is to apply Eq. (8) for different values of M_r of E. It is somewhat tedious but possible. The other way is to go back to the magnetic dynamic equation of motion (after linearization).

$$\frac{1}{\gamma}\frac{\mathbf{dm}}{dt} = \mathbf{M_0} \times \mathbf{h} + \mathbf{m} \times \mathbf{H_0}, \tag{10}$$

where m is the microwave dynamic magnetization, M_0 is the average static internal magnetization = M_r, h is the microwave magnetic field, and H_0 is the static internal field = H_ϕ. The ME coupling to the magnetic motion modifies the above equation

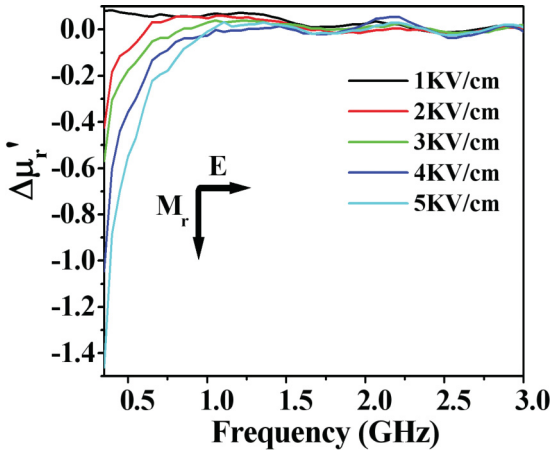

FIG. 5. (Color online) Magnetic permeability change versus electric field over a microwave frequency range when **M** is perpendicular to **E**.

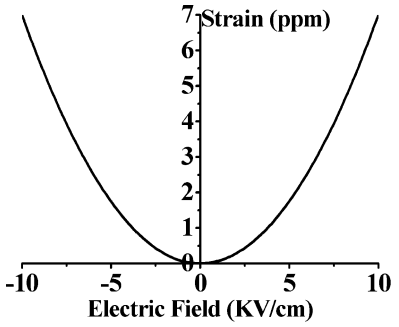

FIG. 6. Electrostriction strain of polycrystalline Sr Z-type versus electric field.

to

$$\frac{1}{\gamma}\frac{\mathbf{dm}}{dt} = \mathbf{M_0} \times \mathbf{h}\left(1 + \frac{\alpha\chi_e(\omega)Z_0}{\chi_e(0)\chi_m(0)}\right) + \mathbf{m} \times \mathbf{H_0}, \qquad (11)$$

where α is the ME coupling $\simeq 0.5 \times 10^{-2}$,[5] $\chi_e(0)$ is the dc electric susceptibility, $\chi_m(0)$ is the dc magnetic susceptibility, and Z_0 is the characteristic impedance of the medium. The ME effect manifests itself as a change in the dynamic magnetic field at microwave frequencies. After much algebra as developed in Ref. 14, we obtain

$$\frac{\Delta\mu_r'}{\mu(0)} \simeq \left(\frac{\chi_m'(f)}{\chi_m(0)} \cdot \frac{\Delta M_r}{M_r}\right)\left(\frac{\chi_e'(f)}{\chi_e(0)} \cdot \alpha Z_0\right), \qquad (12)$$

where $\chi_m'(f)$ and $\chi_e'(f)$ are the real parts of the magnetic and electric susceptibilities, respectively. For example, the complex magnetic susceptibilty is defined as $\chi_m(f) = \chi_m'(f) + i\chi_m''(f) = \frac{4\pi M_r H_1}{H_1 H_2 - \omega^2/\gamma^2}$,[14] where $H_1 = H_\phi + H_\theta, H_2 = H_\phi, \gamma = 2\pi g 1.4 \times 10^6 Hz/Oe, \omega = 2\pi f$, and M_r is the remanence magnetization. Magnetic damping may be included in the expression for $\chi_m(f)$ by assuming ω to be complex. M_r, H_θ (uniaxial magnetic anisotropy field), H_ϕ (six-fold magnetic anisotropy field), and g factor were measured[11] and their corresponding values were 105 G, 25 KOe, 40 Oe, and ~2, respectively. The zero magnetic field FMR frequency, f_0, may be easily deduced from the expression for $\chi_m(f)$ as $f_0 = \frac{\gamma}{2\pi}\sqrt{H_1 H_2} = g1.4 \times 10^6\sqrt{H_\phi(H_\phi + H_\theta)} \simeq 2.51$ GHz. Clearly, f_0 is well above the frequencies where $\Delta\mu_r'(f)$ is maximum ($\lesssim$0.5 GHz). Thus, there is no correlation between the zero magnetic field FMR and $\Delta\mu_r'(f)$, but according to Eq. (7) there is a direct correlation between $\Delta\mu_r'(f)$ and ΔM_r induced by the application of an E field.[11] The relationship between E and ΔM_r is given as $\Delta M_r = \alpha E$, where α is the linear ME coupling. ΔM_r also implies an internal change in magnetization via the spin spiral reconfigurations. Since $\Delta\mu_r'$ is maximum at relatively low frequencies compared to f_0, we can approximate Eq. (7) by neglecting magnetic damping. Magnetic loss or damping is maximum at FMR frequency,

$$\frac{\Delta\mu_r'}{\mu(0)} \simeq \left[\left(\frac{H_\phi H_1}{H_\phi H_1 - \omega^2/\gamma^2}\right)\frac{\Delta M_r}{M_r}\right]\left(\frac{\alpha Z_0}{1 + \omega^2\tau^2}\right), \qquad (13)$$

where ω is real (no magnetic damping), τ is the electric relaxation time, and Z_0 is the characteristic impedance of the ME medium ($\simeq$250). Thus, Eq. (8) is applicable for frequencies below f_0. From Eq. (8), it is predicted that the decrease or "roll-off" of $\Delta\mu_r'(f)$ with frequency is due to electric damping or relaxation rather than magnetic damping. The experimental data in Fig. 4 are compared with the theoretical plot of $\Delta\mu_r'(f)$ as a function of frequency and $E = 5$ KV/cm. Other theoretical plots scale the same with frequency at other values of E. The relaxation parameter τ was assumed to be 3.2×10^{-10} s, which compares with the $\tau \simeq 1.5 \times 10^{-10}$ s deduced from the measured frequency dependence of ϵ (see data in Refs. 4 and 11). Assuming that $\alpha = 60 \times 10^{-4}, Z_0 \simeq 250\ \Omega$, and $\frac{\Delta M_r}{M_r} = 0.16$, we estimate $\Delta\mu_r'(0) = 0.96$, compared to the experimental value of $\simeq$1.2 at $E = 5$ KV/cm.

Finally, in Fig. 6 the strain induced by an electric field is exhibited as a function of the electric field. The strain is quadratic in the electric field strength, which indicates that $Sr_3Fe_{24}Co_2O_{41}$ is neither ferroelectric nor piezoelectric material. Hence, the material exhibits electrostriction, and therefore, it may not be classified strictly as a multiferroic material.

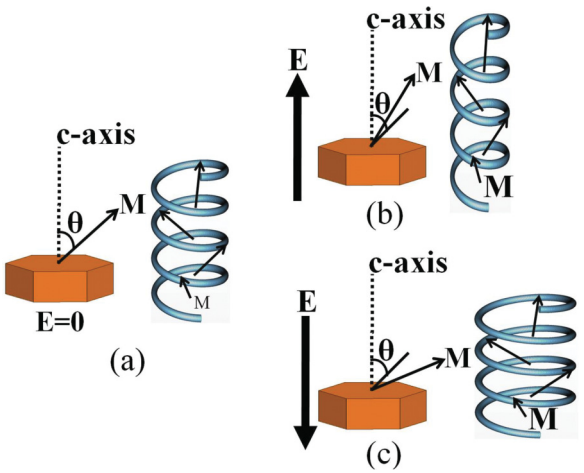

FIG. 7. (Color online) Spin spiral configuration for different directions of E. (a) $E = 0$, (b) E parallel to M, and (c) E antiparallel to M.

III. CONCLUSION AND DISCUSSION

The material hexaferrite $Sr_3Fe_{24}Co_2O_{41}$ exhibits broken symmetries for both time reversal and parity. This is a central feature of these ME materials. Measurements have been made in order to verify this feature, but in a novel manner. The measurements involve the magnetic permeability and strain, both as a function of the electric field **E**. The field dependence on strain indicates that the material is electrostrictive, which distinguishes this material from a pure multiferroic material.

The application of an electric field induces a change in the spin spiral configuration of the hexaferrite via electrostriction. This spin reconfiguration manifests itself as a change in the remanence magnetization ΔM_r and, therefore, as a change in the permeability. The changes in ΔM_r were confirmed by vibrating sample measurements, and changes in permeability were measured using a modified coaxial line technique. This physical picture may be detailed in a sketch we refer to as the "slinky" model (see Fig. 7). With the application of E the angle θ or the angle of the spin within the cone is affected by the direction of E. As the angle θ is varied with E, the size of the "slink" changes, as well as the "net" internal magnetization along E and, therefore, M_r.

It is well known that hexaferrites are mechanically hard along the Caxis and easier to strain in the azimuth plane (perpendicular to the C axis). Figure 6 represents the average strain along the component of **E** in the azimuth plane rather than along the C axis, since the hexaferrite is polycrystalline. Figure 7 shows the average change in magnetization along the component of **E** in the C axis of each crystallite, in agreement with Fig. 4. Hence, the strain along the C axis or the change in magnetization is not at all correlated with the strain as measured in Fig. 6.

As such, from practical considerations this simplifies the design of ferrite devices and applications, since μ is the principal quantity that governs the performance of a microwave ferrite device, for example. Hence there would be less need for permanent magnets in microwave device applications, since only E is applied.

ACKNOWLEDGMENTS

This work was supported by National Science Foundation Grant DMR 1002543.

*Corresponding author: xebat1979@gmail.com

[1] M. Fiebig, J. Phys. D **38**, R123 (2005).
[2] G. Srinivasin, V. Zavislyak, and A. S. Tatarenko, Appl. Phys. Lett. **89**, 152508 (2006).
[3] T. Kato, H. Mikami, and S. Noguchi, J. Appl. Phys. **108**, 033903 (2010).
[4] M. Soda, T. Ishikura, H. Nakamura, Y. Wakabayashi, and T. Kimura, Phys. Rev. Lett. **106**, 087201 (2011).
[5] Y. Kitagawa, Y. Hiraoka, T. Honda, T. Ishikura, H. Nakamura, and T. Kimura, Nature Mater. **9**, 797 (2010).
[6] Y. Takada, T. Nakagawa, M. Tokunaga, Y. Fukuta, T. Tanaka, and T. A. Yamamoto, J. Appl. Phys. **100**, 043904 (2006).
[7] W. Martienssen (ed.), *Landolt-Börnstein: Numerical Data and Functional Relationships in Science and Technology* (Springer-Verlag, Berlin, 1970).
[8] C.-G. Duan, J. P. Velev, R. F. Sabirianov, Z. Zhu, J. Chu, S. S. Jaswal, and E. Y. Tsymbal, Phys. Rev. Lett. **101**, 137201 (2008).
[9] L. D. Landau and E. M. Lifshitz, *Electrodynamics of Continuous Media* (Pergamon Press, Oxford, UK, 1984).
[10] O. Kimura, M. Matsumoto, and M. Sakakura, J. Am. Ceram. Soc. **78**, 2857 (1995).
[11] K. Ebnabbasi, Y. Chen, A. Geiler, V. Harris, and C. Vittoria, J. Appl. Phys. **111**, 07C719 (2012).
[12] A. Widom, S. Sivasubramanian, C. Vittoria, S. Yoon, and Y. N. Srivastava, Phys. Rev. B **81**, 212402 (2010).
[13] L. D. Landau and E. M. Lifshitz, *Electrodynamics of Continuous Media* (Elsevier Butterworth-Heinemann, MA, 1984).
[14] C. Vittoria, *Magnetics, Dielectrics, and Wave Propagation with MATLAB Codes* (CRC Press, New York, 2011).